Adaptive Power Oscillation Damping Controller of Superconducting Magnetic Energy Storage Device for Interarea Oscillations in Power System

Wei Yao[a,b], L. Jiang[b,*], Jiakun Fang[c], Jinyu Wen[a], Shijie Cheng[a], Q. H. Wu[b]

[a]*State Key Laboratory of Advanced Electromagnetic Engineering and Technology, Huazhong University of Science and Technology, Wuhan, 430074, China.*
[b]*Department of Electrical Engineering and Electronics, University of Liverpool, Liverpool, L69 3GJ, United Kingdom*
[c]*Department of Energy Technology, Aalborg University, 9220 Aalborg, Denmark*

Abstract

This paper presents an adaptive power oscillation damping (APOD) scheme for the superconducting magnetic energy storage (SMES) device to suppress the interarea oscillation in the inter-connected power system. The APOD scheme is designed based on the generalized predictive control (GPC) and model identification approaches. A recursive least-squares algorithm (RLSA) with a varying forgetting factor is utilized to identify a reduced-order model of the power system online. Based on this identified model, the GPC scheme considering control output constraints can yield an optimal control action by performing an optimization procedure over a prediction horizon. Owing to the usage of the RLSA, the proposed APOD controller can effectively adapt to the variations of operating conditions and parameter uncertainties of the power system. Case studies are undertaken on the New England 10-machine 39-bus power system. Simulation results verify the proposed APOD can consistently provide better damping performance than that

*Corresponding Author: L. Jiang, Tel.: +44 151 7944509, Email: ljiang@liv.ac.uk

of the conventional lead-lag POD, over a wide range of operating conditions and different disturbances.

Keywords: Superconducting magnetic energy storage (SMES), generalized predictive control, adaptive control, power oscillation damping (POD) controller, model identification.

---

1. Introduction

Interarea oscillations are often observed from the tie-lines between control areas when the interconnected large-scale power systems are suffered from disturbances such as faults, line outages and sudden load changes [1]. These power oscillations must be well suppressed to ensure the secure operation and stability of the power system after disturbances [2, 3]. Conventionally, the power system stabilizers (PSSs) installed at the generators [4, 5] and supplementary damping controller designed for the flexible AC transmission systems (FACTS) devices are used to damp these power oscillations [6, 7, 8]. Alternatively, superconducting magnetic energy storage (SMES) device, which is capable of swiftly exchanging active and reactive power with the power system, has been suggested by many researchers to damp out power system oscillations, because the power oscillations can be more effectively suppressed through active power modulation [9, 10, 11, 12].

To damp out the interarea oscillations effectively, many control techniques have been applied for the design of power oscillation damping (POD) controller for the SMES device, which plays a crucial role on the damping performance of the closed-loop system. Traditionally, the proportional-integral (PI) or lead-lag controllers have been employed, which can provide satisfactory damping perfor-

mance around a specific operating condition [9]. The drawback of those POD controllers is that the usage of the fixed parameters may degrade performance when the system operating condition changes. To improve the performance of the POD controller, various advanced control methods have been implemented, such as robust control [11, 13, 14, 15, 16], the energy function-based controller [17] and the lead-lag controller with anti-windup compensator [18]. However, most of those controller designs require a mathematical model of the power system, which is very difficult or even unfeasible for a practical large-scale power system. An alternative solution is a measurement-based design.

Model identification techniques have been applied to obtain an equivalent model online for designing adaptive controllers for the power system, which is based on input-output measurements and capable of coping with the model variation of the power system [4, 19, 20, 21]. On the other hand, the generalized predictive control (GPC) is one of the major optimal control strategies and has received a great deal of attention as a powerful tool for the control of industrial process systems [22, 23, 24]. It has been proved that the GPC approach can not only deal with variable dead-time, but also cope with over-parameterization [24]. Moreover, the main feature of the GPC compared with other control methods is the explicit inclusion of system constraints in the controller formulation [22]. The GPC has been applied successfully to power system showing good performance and certain degree of robustness, such as design of controllers for FACTS devices [25, 26] and the generator excitation system [5, 23, 27].

In this paper, an adaptive POD (APOD) controller is designed for the SMES device to improve the damping of interarea oscillation in the power system, based on the GPC and model identification techniques. The proposed APOD controller

yields an optimal control action by performing an optimization procedure over a prediction horizon in each sampling interval. Owing to the usage of the model identifier, the proposed APOD controller can effectively deal with the unmodeled dynamics such as variations of operating conditions, parameter uncertainties and different scale of the power system. Simulation tests are carried out based on the New England 10-machine 39-bus power system. Simulation results demonstrate the effectiveness of the proposed APOD controller over a wide range of operating conditions and different disturbances.

The remainder of this paper is organized as follows: the New England 10-machine 39-bus test system is presented in Section II. Section II gives a brief description of the proposed adaptive POD control scheme. Section IV designs an APOD controller for the SMES by using the adaptive GPC scheme, and the simulation results are reported in Section V. Section VI presents the conclusions of this work.

2. Test System

The New England 10-machine 39-bus power system, shown in Fig. 1, is used as the test system. It consists of 10 machines, 39 buses, and 46 lines, and its detailed parameters are given in [30]. It has been widely used as a test benchmark for studying the low frequency oscillations as it performs several interarea modes under disturbances or faults. The tie-lines of the New England power system are the lines connecting bus 16-17 and 16-15. The outages of these tie-lines have a significant impact on the damping and frequency of the interarea modes. Each of the generators is represented by a fourth-order model and equipped with an IEEE ST1A excitation system. All the transmission systems are modeled as passive

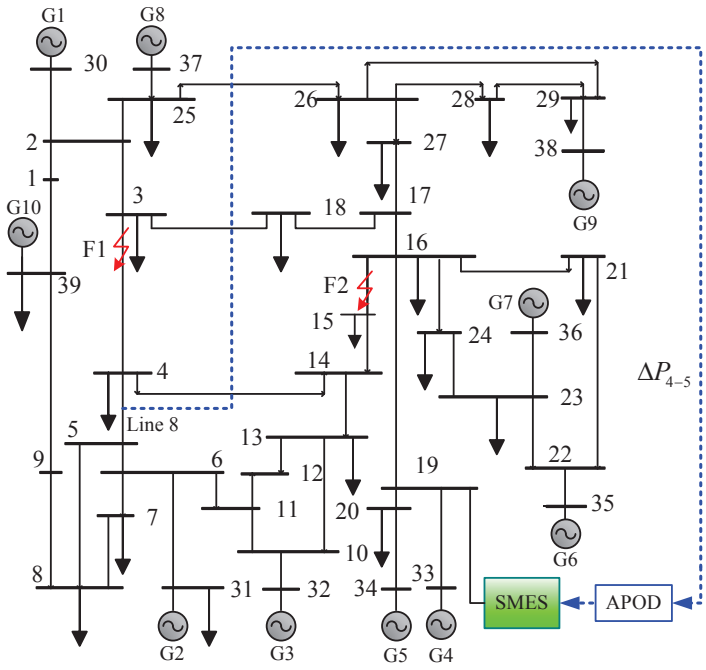

Figure 1: Single line diagram of the New England power system with an SMES device

circuits while the loads are considered as constant impedances. The output of the mechanical power of each generator is treated as a constant value for simplicity.

The nonlinear model of the New England 39-bus power system is linearized at a nominal operating condition [30]. The modal analysis results of the interarea modes of this test system without PSS and with several PSSs are given in Table 1. Since the test system without PSS has two modes with negative damping ratios, several PSSs are added to generators to improve the stability of the system. It can be found that this system with several PSSs still has an interarea mode whose damping ratio is less than 0.05. Compared with the Mode 1, Modes 2 and 3 have relatively higher frequencies and larger damping ratios. Therefore, the objective is to design a POD controller to produce robust damping for the critical Mode 1, as

Table 1: Interarea oscillation modes of the test system (With PSS means G1, G3, G4, G7, G8, G9 equipped with PSS)

Mode Index	Mode Type	Without PSS		With PSS	
		ξ	f (Hz)	ξ	f (Hz)
1	Inter-area	-0.0130	0.6311	0.0442	0.6273
2	Inter-area	-0.0224	0.9640	0.0556	0.9368
3	Inter-area	0.0059	1.0409	0.0677	1.0561

it has smallest damping ratio 0.0442 and lowest oscillation frequency 0.6273Hz.

In order to damp out power system oscillation caused by the occurrence of fault, a ±300MW SMES device is installed at bus 19 [18]. The response of the SMES is assumed to be very fast and is modeled by a single time constant [11]. The detailed control scheme of the SMES device is depicted in Fig. 2 and its parameters are given in [11]. It is a simultaneous active and reactive power control scheme, which includes POD controller and voltage regulator. The POD controller and voltage regulator are the active and reactive power controllers of the SMES device, respectively. In this paper, it is assumed that for the steady state the SMES devices do not deliver or absorb active power to/from the power system but their respective reactive power control loop is always closed to provide reactive power support within the limit. On the other hand, the SMES device should alleviate power system oscillations when subjected to system disturbances.

3. Adaptive POD Control Scheme

The basic principle of the APOD control scheme for the SMES device is depicted in Fig. 3. The APOD scheme is an indirect type controller and consists of

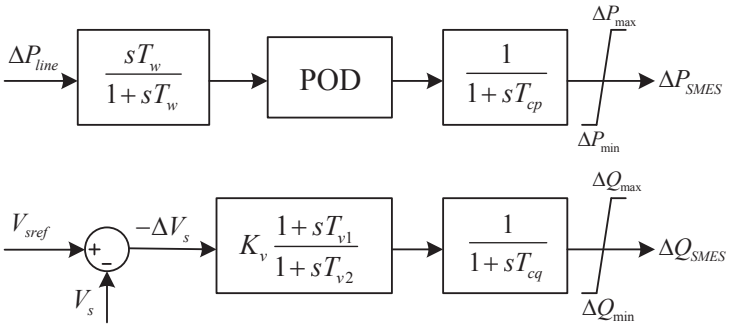

Figure 2: Block diagram of the control scheme of an SMES device

two parts: online model identification and synthesis of the controller by the GPC technique. In every sampling interval, the model identifier updates the parameters of the reduced low-order model of the power system according to the past input/output sequences. The updated low-order model is then used for the predictive model of the GPC controller to generate an optimal control signal to meet the specific control requirements.

The GPC is usually developed based on a controlled auto-regressive integrated moving average (CARIMA) model, which is an incremental model. The reason for using this model is that many control situations require a nonzero steady-state control signal, which is achieved by penalizing $\Delta u(t)$ in the GPC cost function. However, the control signal, which has a nonzero offset after the occurrence of a perturbation in the system, is not allowed in the SMES damping controller applications [27]. Therefore, in order to avoid the offset of the control signal, the following controlled auto-regressive and moving average (CARMA) model is utilized to design an APOD for the SMES device.

$$A(z^{-1})y(t) = B(z^{-1})u(t-1) + C(z^{-1})e(t) \tag{1}$$

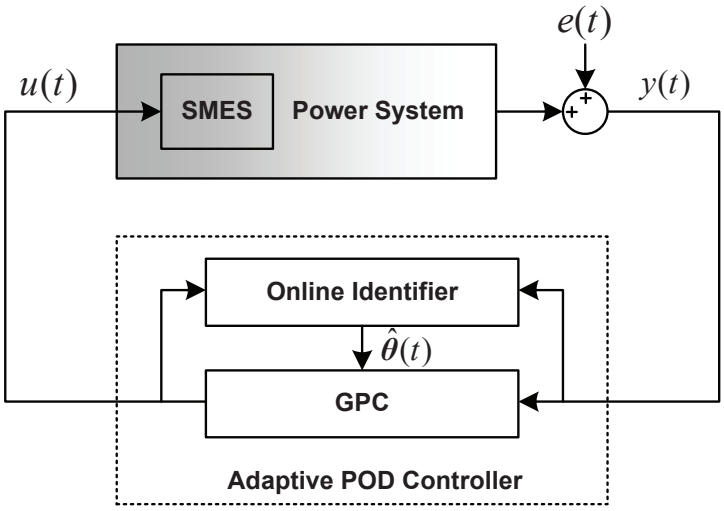

Figure 3: Block diagram of the adaptive POD controller for the SMES device

where

$$A(z^{-1}) = 1 + a_1 z^{-1} + \ldots + a_{n_a} z^{-n_a}$$
$$B(z^{-1}) = b_0 + b_1 z^{-1} + \ldots + b_{n_b} z^{-n_b}$$
$$C(z^{-1}) = 1 + c_1 z^{-1} + \ldots + c_{n_c} z^{-n_c}$$

$y(t)$, $u(t)$, and $e(t)$ are the system output, system input, and discrete white noise, respectively. $A(z^{-1})$, $B(z^{-1})$, and $C(z^{-1})$ are n_a, n_b, and n_c order polynomial, respectively. Also z^{-1} denotes the backward shift operator, for example, $z^{-1}y(t) = y(t-1)$. The polynomial $C(z^{-1})$ may either represent the external noise components affecting the output or a design polynomial interpreted as a fixed observer for the prediction of future outputs. For simplicity, the $C(z^{-1})$ polynomial is usually chosen to be 1.

3.1. Online Model Identification

For the design of POD controller, a simple low-order CARMA model with fixed structure shown in (1) but whose parameters vary with the operating conditions, is proposed to represent the dynamic oscillations in the power system [27, 21]. This low-order model is sufficient to represent the power system for the control design problems, even if a practical power system is a complex nonlinear and high-order dynamic system [5]. A recursive least-squares algorithm (RLSA) with a varying forgetting factor is used to estimate parameters a_i and b_i of the CARMA model [4]. A general formulation is presented in the sequel.

Given the vector $\widehat{\theta}(t)$ of parameter estimates by:

$$\widehat{\theta}(t) = \left[\begin{array}{cccccccc} a_1, & \ldots & a_{n_a}, & b_0, & b_1, & \ldots & b_{n_b} \end{array} \right]^T \tag{2}$$

and measurement vector $\phi(t)$ by:

$$\phi(t) = [-y(t-1), \ldots, -y(t-n_a), u(t-1), \ldots, u(t-n_b-1)]^T \tag{3}$$

The update of the estimates is obtained by:

$$\left\{ \begin{array}{ll} \eta(t) & = y(t) - \phi^T(t)\widehat{\theta}(t-1) \\ K(t) & = P(t-1)\phi(t)/[1 + \phi^T(t)P(t-1)\phi(t)] \\ \widehat{\theta}(t) & = \widehat{\theta}(t-1) + K(t)\eta(t) \\ \lambda(t) & = 1 - [1 - \phi(t)^T K(t)]\eta(t)^2/\Sigma_0 \\ P(t) & = [I - K(t)\phi^T(t)]P(t-1)/\lambda(t) \end{array} \right. \tag{4}$$

where $P(t)$ is the covariance matrix, I identity matrix, $K(t)$ adjustment gains, $\lambda(t)$ the time-varying forgetting factor used to improve the parameter track accuracy of the identifier, and Σ_0 is the preselected constants, which can be determined by using the method proposed in [4].

In addition, to protect parameters from large modeling errors caused by the suddenly large disturbance, moving boundaries are introduced for every parameter to avoid which undesired rapid parameter fluctuations. This is particularly critical in power systems, where a variety of suddenly large disturbances (fault) occur [20]. The mean values of the estimated parameters at the instant t are of the form:

$$\beta_i(t) = \frac{1}{T}\sum_{k=1}^{T}\theta_i(t-k) \quad i = 1, 2, ..., (n_a + n_b + 1) \tag{5}$$

where $\theta_i(t)$ is the element in $\widehat{\theta}(t)$, and $T > 1$, with a value chosen to ensure stability of the parameters. The larger the value of the T, the more stable and less adaptable the parameter boundaries become.

The high and low boundaries for each parameter are defined as follows:

$$\begin{cases} \beta_{iH}(t) = \beta_i(t) + \gamma|\beta_i(t)| \\ \beta_{iL}(t) = \beta_i(t) - \gamma|\beta_i(t)| \end{cases} \tag{6}$$

where $0 < \gamma < 1$, the larger the value γ, the more likely it is for the parameters to vary. At each sampling instant, each estimated parameter is bounded by its corresponding high and low boundaries.

3.2. Generalized Predictive Control

Once the parameters of the model are properly estimated in each sampling interval, the GPC algorithm is adopted to generate the optimal control signal. Since the design of an APOD controller for the SMES device is a regulation problem, the output reference $y_r(t + j) \equiv 0$. Consequently, the quadratic cost function to be minimized is defined as follows:

$$J(N, N_u) = E\left\{\sum_{j=1}^{j=N}\widehat{y}(t+j)^2 + \sum_{j=1}^{j=N_u} r_j u(t+j-1)^2\right\} \tag{7}$$

where $E\{.\}$ is the expectation operator, $\widehat{y}(t+j)$ is an optimal j-step ahead prediction of the system output up to time t, $y_r(t+j)$ is the reference for the output. N is the prediction horizon, $u(t+j-1)$ is an optimal j-step ahead prediction of the system input, N_u is the control horizon, r_j is a control weighting sequence and usually defined as a constant value, $r_j = r$, for $j = 1, 2, ..., N_u$.

By solving the Diophantine equations, the N j-ahead predictions can be represented by the following matrix equation [24]:

$$\hat{y} = GU + f \tag{8}$$

where

$$\begin{aligned}
\hat{y} &= \begin{bmatrix} \hat{y}(t+1) & \hat{y}(t+2) & ... & \hat{y}(t+N) \end{bmatrix}^T, \\
U &= \begin{bmatrix} u(t) & u(t+1) & ... & u(t+N_u-1) \end{bmatrix}^T, \\
f &= \begin{bmatrix} f_1 & f_2 & ... & f_N \end{bmatrix}^T, \\
G &= \begin{bmatrix} g_0 & 0 & \cdots & 0 \\ g_1 & g_0 & \cdots & 0 \\ \vdots & \vdots & \ddots & \vdots \\ g_{N_u-1} & g_{N_u-1} & \cdots & s_0 \\ \vdots & \vdots & \ddots & \vdots \\ g_{N-1} & g_{N-2} & \cdots & s_{N-N_u} \end{bmatrix}, \\
s_i &= \sum_{j=0}^{i} g_j.
\end{aligned}$$

The elements g_i of the matrix G, with dimensions $N \times N_u$, are points of the plant's step response and can be computed recursively from the model. The elements f_i of the matrix f can be computed similarly.

One of the major advantages of the GPC is its ability to handle constraints online in a systematic way, since the algorithm does this by optimizing predicted

performance subject to constraint satisfaction. In practice, the constraints of the control signal $u(t)$ should be considered and can be expressed as follows:

$$u_{\min} \leq u(t) \leq u_{\max} \tag{9}$$

where $u_{\min}$ and $u_{\max}$ denote the lower limit and upper limit of the control signal. Thus,

$$\Gamma u_{\min} \leq U \leq \Gamma u_{\max} \tag{10}$$

where Γ denotes the N_u identity vector.

According to the (7) and (10), the implementation of GPC with bounded signals can be represented as a quadratic programming (QP) problem. That is an optimization problem with a quadratic objective function and linear constraints. This inequality constrained QP problem can be stated as:

$$\begin{aligned} \min \quad & J(U) = \tfrac{1}{2} U^T H U + b^T U + f_0 \\ \text{s.t.} \quad & A_{\text{qb}} U \leq b_c \end{aligned} \tag{11}$$

where $H = 2(G^T G + R)$, $R = [r_1, r_2, ..., r_{N_u}]$, $b = 2f^T G$, $f_0 = f^T f$, $A_{\text{qb}} = [I, -I]^T$, and $b_c = [\Gamma u_{\max}, -\Gamma u_{\min}]^T$. I is the identity matrix.

The control signal $U = [u(t) \;\; u(t+1) \;\; ... \;\; u(t+N_u-1)]^T$ can be obtained by solving the above QP problem. Since the GPC is a receding-horizon control method, only the first row of U is actually applied at each sampling interval.

4. Design of Adaptive POD Controller

For the design of the POD controller for the SMES device, the selection of the SMES controller location and the input signal is an essential issue. To select the optimal location and best input signal for the controller, the geometric measures

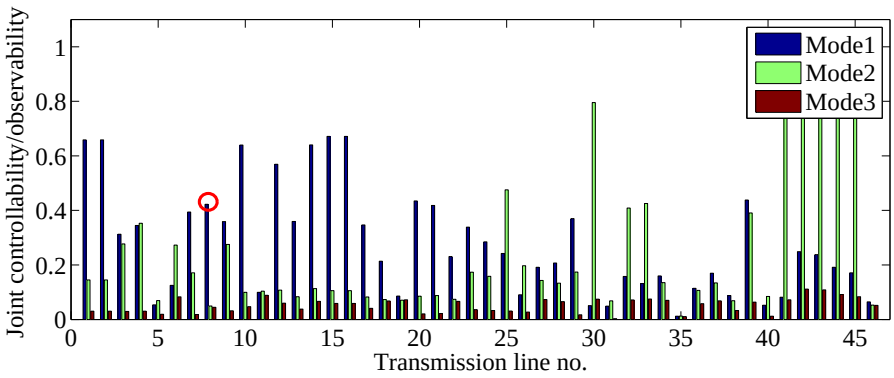

Figure 4: The joint geometric controllability/observability of different transmission lines with respect to Mode 1, 2, 3

of controllability/observability from [2, 18, 28, 29] are used in this paper. To avoid interfering other modes, the wide-area feedback signal, which has relatively large joint geometric controllability/observability with respect to critical mode and relatively smaller joint geometric controllability/observability with respect to other modes, should be chosen as the stabilizing signals of the POD controller. The joint geometric controllability/observability of different transmission lines with respect to Mode 1, 2, 3 are shown in Fig. 4. It can be found that the active power of the line 8 (P_{4-5}, indicated by a red circle as shown in Fig. 4) has larger joint geometric controllability/observability with respect to Mode 1 and has the smallest joint geometric controllability/observability with respect to Mode 2 and 3. Therefore, the P_{4-5} is selected as the stabilizing signal of the POD controller in this paper. Furthermore, to avoid the ill-conditioned estimation problem, the wide-area signal ΔP_{4-5} (p.u) is scaled to $0.2\Delta P_{4-5}$. In addition, a washout filter is added to eliminate constant deviation of ΔP_{4-5} when the operating condition of the system is changed.

The linear model shown as (1) is used for the prediction model of the APOD controller. Obviously, a higher-order model means more calculations for the identifier and the controller. The reduced odd order models, which can capture the essential dynamics, could be proposed to represent the dynamic oscillations in the power system and it is sufficient to represent the low frequency power oscillations. This is because the reduced odd order model has several pairs of complex poles and a real pole. The complex poles represent the oscillatory behavior of the power oscillations, whereas the real root represents the decaying part of the oscillatory response. In this paper, the order of the linear model is chosen to be: $n_a = 3$, $n_b = 3$.

For the proposed APOD controller, the sampling period $T_s = 100$ms is determined based on the frequency of the critical interarea Mode 1. The following parameters need to be specified for the proposed APOD controller: the prediction horizon N, the control horizon N_u, the weighting sequence r. Although their values are normally guided by heuristics, there are some general guidelines for choosing these parameters to ensure the optimization is well proposed in [5, 24]. Generally speaking, the prediction horizon N should be greater than the N_u and the system settling time. In this paper, N is chosen to be $N = 25$, as no perceptible additional improvement is verified for larger values. For the control horizon N_u, a conservative choice of N_u is that the N_u is at least equal to the number of unstable or badly-damped poles, this choice allows the good control performance can be achieved. Thus, N_u is chosen to be $N_u = 5$ because any further increase in N_u makes little difference in system performance. The control weighting r should be chosen so that the magnitudes of the control terms are of a similar order as the tracking terms. In this study, r is chosen as $r = 8.2e - 4$ by the trial-and-error

method. In addition, the parameters of the identifier are chosen as: $\Sigma_0 = 0.02$, $T = 10$, $\gamma = 0.05$. According to the capacity of the installed SMES device, ±3 pu (±300MW SMES) is limited to the output of the adaptive POD controller.

5. Simulation Studies

To verify the validity and effectiveness of the adaptive POD controller of the SMES device, simulation studies are carried out based on the New England 10-machine 39-bus power system shown in Fig. 1. For comparison, the conventional POD (CPOD) controller of the SMES device designed by using residue method given in [1] is also investigated. The transfer function of the 7^{th} reduced-order model of the test system obtained from the original model by using the Schur model reduction method [29] is given in Appendix, while the transfer function of the CPOD controller is given as follows,

$$H_{\text{POD}}(s) = 0.3\frac{10s}{1+10s}\left(\frac{1+0.5748s}{1+0.1120s}\right)^2 \tag{12}$$

The root locus of the closed-loop power system with the CPOD controller is shown in Fig. 5. When K_{POD} changes from 0 to 1.0, the damping ratio of the Mode 1 increases significantly, whereas the damping ratios of both Modes 2 and 3 change very slightly. It reveals that the interactions of the POD with other modes are tiny. This also proves the validity of the feedback signal selection in the last Section.

In this paper, simulation tests are carried out considering the following three typical fault scenarios:

Scenario I: Under the nominal operating condition, active power of tie-lines is 493MW, a three-phase-to-ground fault (Fault F1 shown in Fig. 1) occurs at the

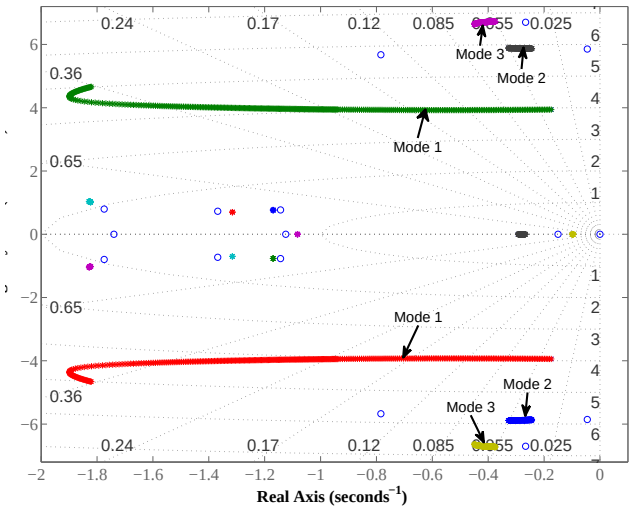

Figure 5: The root locus of the closed-loop New England 10-machine 39-bus power system ($K_{\mathrm{POD}} : 0 - 1.0$)

end terminal of line 3-4 near bus 3 at $t = 0.5$s, followed by switching off the faulty transmission line at $t = 0.6$s.

Scenario II: Under the nominal operating condition, active power of tie-lines is 493MW, a three-phase-to-ground fault (Fault F2 shown in Fig. 1) occurs at the end terminal of tie-line 15-16 near bus 15 at $t = 0.5$s, followed by switching off the faulty tie-line at $t = 0.6$s.

Scenario III: Under a heavy operating condition, active power of tie-lines is 884MW, a three-phase-to-ground fault (Fault F1) occurs at the end terminal of line 3-4 near bus 3 at $t = 0.5$s, followed by switching off the faulty transmission line at $t = 0.6$s.

Note that the test system operates at a new operating point during the post-fault period because of the outage of the faulty transmission line, and the scenario

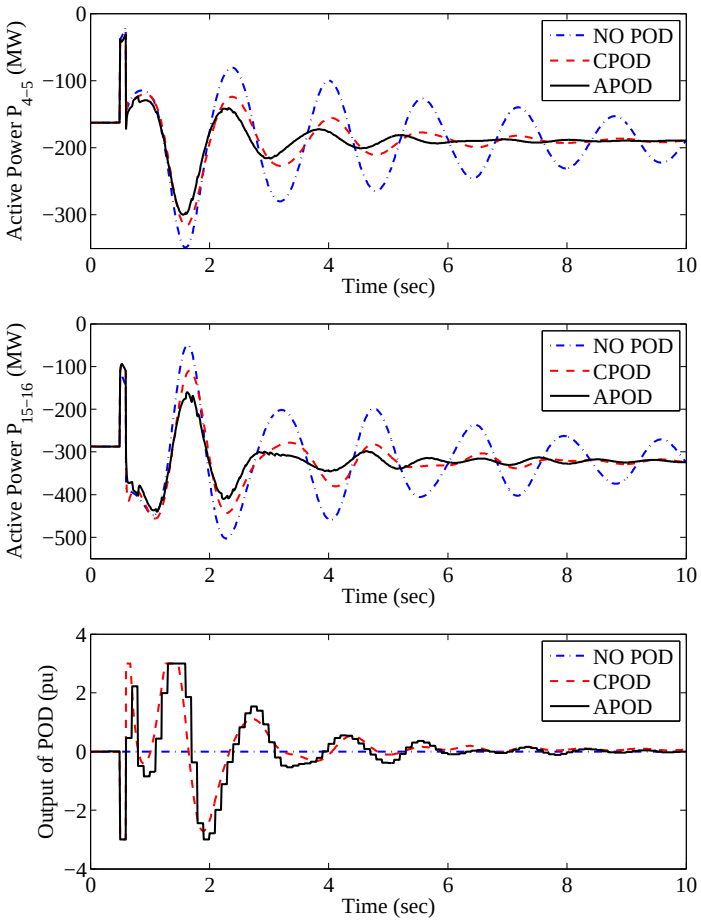

Figure 6: System response to Scenario I (active power of tie-lines is 493MW, fault F1)

II represents a larger change of operating conditions.

Under the fault scenario I, the system performance without POD, with CPOD, and with the proposed APOD is depicted in Fig. 6. It can be found that the performance of a system with APOD is slightly better than that of the system with CPOD. Moreover, both the APOD and CPOD can damp out the critical inter-area oscillation effectively. Note that the CPOD is tuned and tested under this nominal operating condition. It is also proved that the third-order identified model can

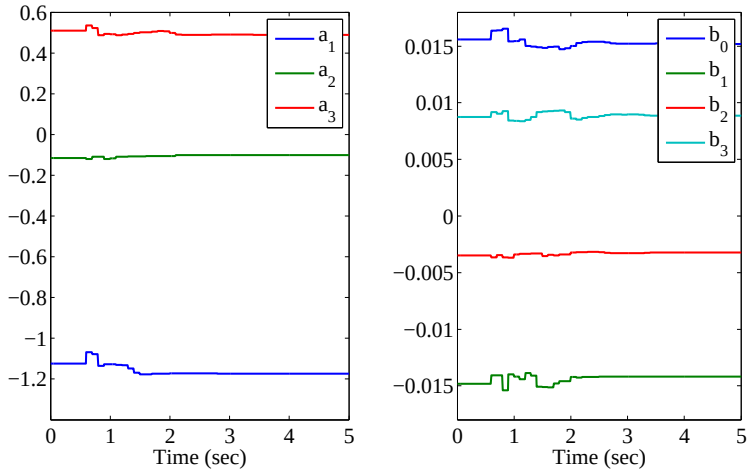

Figure 7: Variation of the identified parameters of the prediction model under Scenario I

track the dynamic of the power system and be utilized for the prediction model of the APOD. In addition, the variations of the identified parameters of the prediction model under this situation are depicted in Fig. 7. It can be found that the identified parameters are updated fast enough to track the change of operating condition and external disturbance. The parameters move to the new steady values during the post-fault period. Furthermore, the identifier equipped with the moving boundaries (6) offers a smooth parameter tracking ability even during a large disturbance as shown in Fig. 7.

Under the fault scenario II, the system performance without POD, with C-POD, and with the proposed APOD is depicted in Fig. 8, and the variations of the identified parameters of the prediction model under this situation are also illustrated in Fig. 9. The scenario II is a severe contingency due to the outage of the tie-line 15-16. The active power of tie-line 16-17 increases from 205MW to 474MW under this fault scenario. The operating condition of the system during

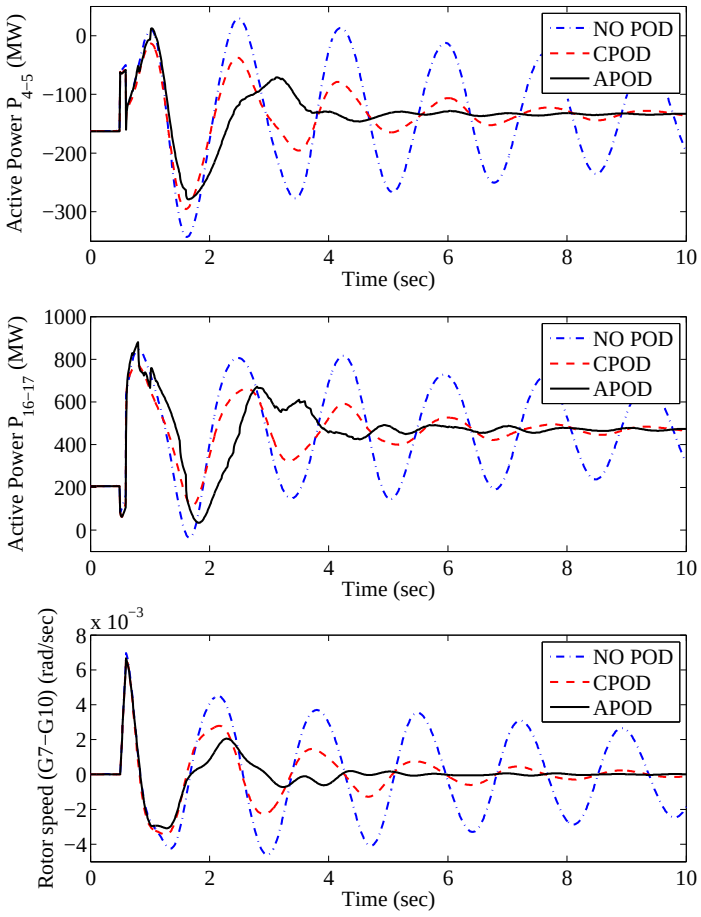

Figure 8: System response to Scenario II (active power of tie-lines is 493MW, fault F2)

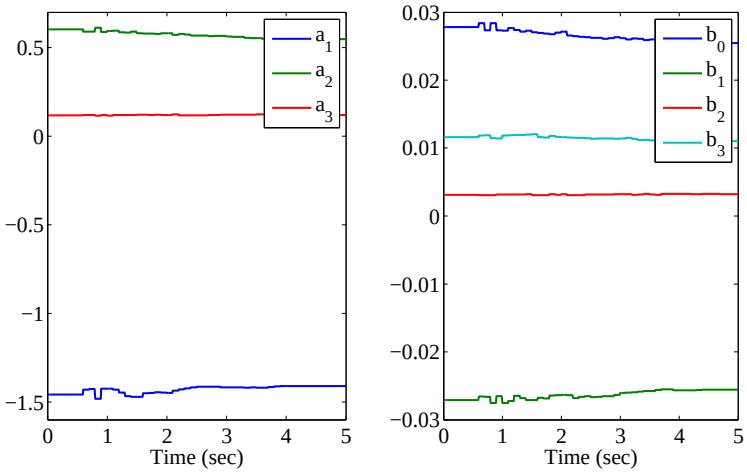

Figure 9: Variation of the identified parameters of the prediction model under Scenario II

the post-fault period is quite different from that of the system during the pre-fault period. It can be seen that the stability of the system without POD deteriorates during the post-fault period. It also reveals that the performance of the system with APOD is better than that of the system with CPOD. These results reveal the fact that, although the CPOD can improve the damping for several operating conditions of the system, it cannot guarantee the same performance for all these conditions. Compared Fig. 9 with Fig. 7, it can be found that the parameters under scenario II need a longer time to converge to a steady state than that of the parameters under scenario I. This is because the post-fault steady state is more different than the pre-fault steady state under scenario II.

When the system is under a heavy operating condition, the system response to fault scenario III are shown in Fig. 10, and the variations of the identified parameters of the prediction model under this situation are also illustrated in Fig. 11. It can be found that the performance of the system with the APOD is much better

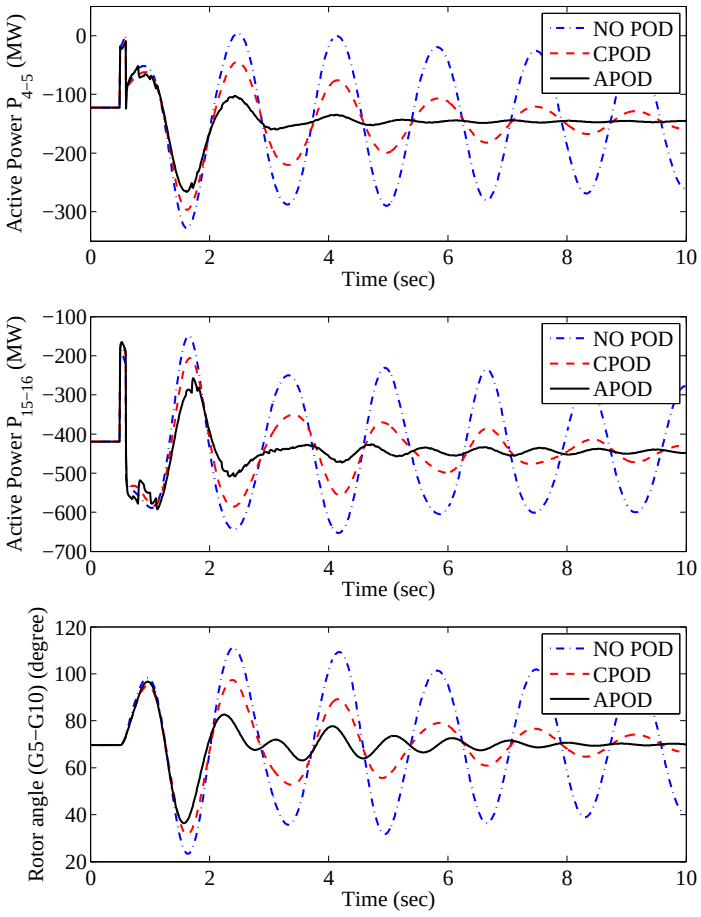

Figure 10: System response to Scenario III (active power of tie-lines is 884MW, fault F1)

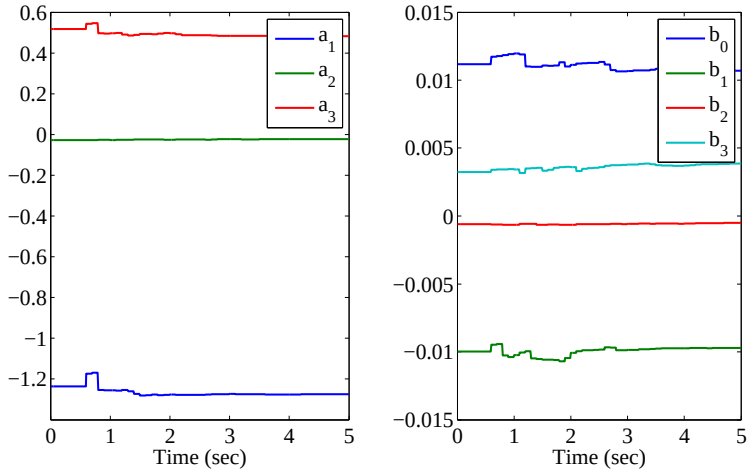

Figure 11: Variation of the identified parameters of the prediction model under Scenario III

than that of the system with the CPOD. That is because the CPOD is tuned based on a specific operating condition and its performance will be degraded when the system operating condition varies, while the APOD can adopt to the variation of the operating condition due to the self-adjustment capability of the model identification scheme.

The damping performance of different SMES capacity under scenario III is also illustrated in Fig. 12. It can be found that the output of the APOD is limited by the SMES capacity. Moreover, the smaller SMES capacity is, the more easily the output of POD reaches to its upper or lower limit. Therefore, the system damping performance will deteriorate with the decrease of the SMES capacity and vice versa. To quantitatively assess the SMES capacity's influence on dynamic performance of the system, the integral of the time multiplied by the absolute error (ITAE) is calculated by [18]

$$J_{\mathrm{ITAE}} = \int_0^{t_{\mathrm{sim}}} t|\Delta P_{4-5}|dt \tag{13}$$

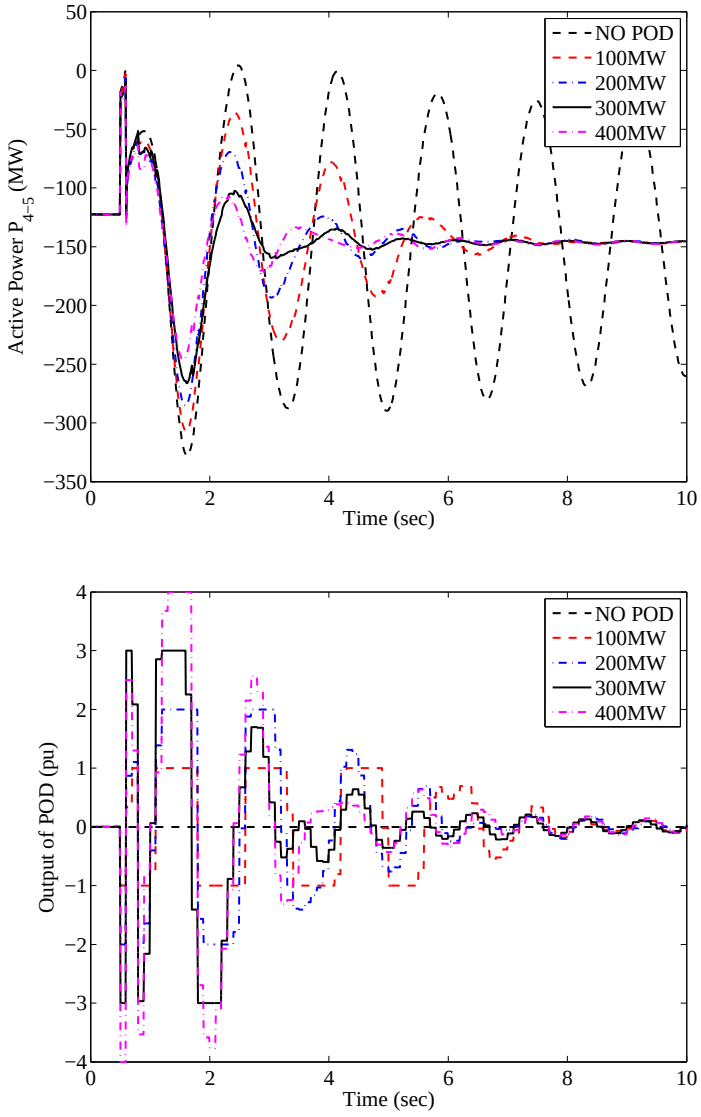

Figure 12: Influence of different SMES capacity on damping performance under Scenario III (active power of tie-lines is 884MW, fault F1)

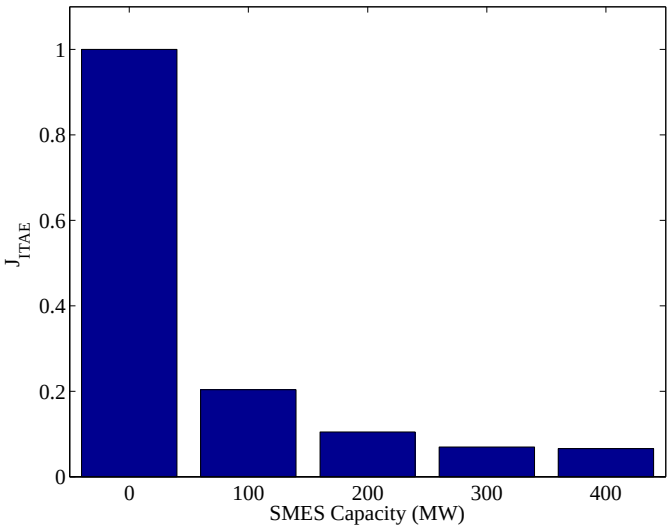

Figure 13: Influence of different SMES capacity on performance index under Scenario III (active power of tie-lines is 884MW, fault F1)

where, ΔP_{4-5} means the active power deviation of the line 4-5, t_{sim} is the simulation time, 10s in this paper. Smaller J_{ITAE} indicates less deviation of synchronousness and shorter time to reach a new steady state, hence a better performance and a more stable the system. Here, the ITAE index is used as the supplement and conclusion to assess the influence of the SMES capacity quantitatively. The influence of different SMES capacity on performance index is illustrated in Fig. 13. For simplification, the ITAE index is normalized so that the largest element is equal to 1. It can be found that a progressive improved performance has been noticed when the SMES capacity is up to 300MW. No obvious additional improvement is verified when the SMES capacity increases to 400MW. When the SMES capacity is lower than 300MW, the damping performance deteriorates gradually. Consequently, the SMES device with the capacity of 300MW is appropriate for stable

operation of the test power system. In addition, the generalized predictive control can deal with the noise properly, since the optimal predictive output is obtained by solving the Diophantine equations [24]. Moreover, since the positional control approach considered in this paper, the measurement noise is not as critical as it would be for an incremental control [27]. This also has been proved in [31]. Therefore, the proposed APOD can still provide a good damping performance in case of measurement noise.

6. Conclusion

Based on generalized predictive control and model identification approaches, an adaptive power oscillation damping (APOD) controller has been designed for the SMES device to damp the interarea oscillation of an interconnected power system. A reduced-order equivalent model of the large-scale power system is identified online by using a recursive least-squares algorithm with a varying forgetting factor, which can adapt to the model uncertainties caused by the variations of the operating condition and faults. Based on the estimated model, the generalized predictive control approach is employed to calculate the optimal control, considering the output constraints of the SMES. The effectiveness of the proposed APOD controller is evaluated by a simulation study on the New England 10-machine 39-bus power system. Compared with the conventional POD controller, the simulation results show that the APOD can consistently provide better damping performance to the interarea oscillation over a wide range of operating conditions and different disturbances. In addition, it is also proved that the reduced-order identified model can track the dynamic of the power system and be utilized for the APOD controller.

Acknowledgments

This work was supported by the National Basic Research Program of China (973 Program) under Grant No. 2012CB215106 and National Natural Science Foundation of China under Grant No. 51428702.

Appendix

The 7$^{\text{th}}$ reduced-order transfer function of the test system is given as follows:

$$G_{\mathrm{P}}(s) = \frac{5.3943(s+0.2713)(s+0.01317)(s^2+0.9671s+35.67)(s^2+1.384s+118.9)}{(s+0.02169)(s+0.4714)(s+94.01)(s^2+0.3491s+15.61)(s^2+1.59s+79.56)}$$

References

[1] P. Kundur, *Power system stability and control*, New York: McGraw-Hill, 1994.

[2] Y. Zhang and A. Bose, Design of wide-area damping controllers for inter-area oscillations, IEEE Trans. Power Syst., 23(2008) 1136-1143.

[3] W. Yao, L. Jiang, J. K. Fang, J. Y. Wen, and S. J. Cheng, Decentralized nonlinear optimal predictive excitation control for multi-machine power systems, Int. J. Electr. Power Energy Syst., 55(2014) 620-627.

[4] S. J. Cheng, Y. S. Chow, O. P. Malik, and G. S. Hope, An adaptive synchronous machine stabilizer, IEEE Trans. Power Syst., 1(1986) 101-107.

[5] B. Wu and O. P. Malik, Multivariable adaptive control of synchronous machines in a multimachine power system,IEEE Trans. Power Syst., 21(2006) 1772-1781.

[6] A. Domahidi, B. Chaudhuri, P. Korba, R. Majumder, and T. C. Green, Self-tuning flexible ac transmission system controllers for power oscillation damping: a case study in real time, IET Gener. Transm. Distrib., 3(2009) 1079-1089.

[7] A. Safari and N. Rezaei, Towards an extended power system stability: An optimized GCSC-based inter-area damping controller proposal, Int. J. Electr. Power Energy Syst., 56(2014) 316-324.

[8] J. D. Nguimfack-Ndongmo, G. Kenne, R. Kuate-Fochie, A. Cheukem, H. B. Fotsin, and F. Lamnabhi-Lagarrigue, A simplified nonlinear controller for transient stability enhancement of multimachine power systems using SSSC device, Int. J. Electr. Power Energy Syst., 54(2014) 650-657.

[9] C. J. Wu and Y. S. Lee, Application of superconducting magnetic energy storage unit to improve the damping of synchronous generator, IEEE Trans. Energy Convers., 6(1991) 573-578.

[10] J. F. Hauer and H. J. Boenig, Control aspects of the Tacoma superconducting magnetic energy storage project, IEEE Trans. Power Syst., 2(1987) 443-450.

[11] B. C. Pal, A. A. Coonick, I. M. Jaimoukha, and H. El-Zobaidi, A linear matrix inequality approach to robust damping control design in power systems with superconducting magnetic energy storage device, IEEE Trans. Power Syst., 15(2000) 356-362.

[12] B. M. Ge, W. L. Wang, D. Q. Bi, C. B. Rogers, F. Z. Peng, A. T. de Almeida, and H. Abu-Rub, Energy storage system-based power control

for grid-connected wind power farm, Int. J. Electr. Power Energy Syst., 44(2013)115-122

[13] Y. Wan and J. Zhao, H_∞ control of single-machine infinite bus power systems with superconducting magnetic energy storage based on energy-shaping and backstepping, IET Control Theory Appl., 7(2013) 757-764.

[14] A.H.M.A. Rahima and E.P. Nowicki, A robust damping controller for SMES using loop-shaping technique, Int. J. Electr. Power Energy Syst., 27 (2005) 465-471.

[15] I. Ngamroo and S. Vachirasricirikul, Coordinated control of optimized SF-CL and SMES for improvement of power system transient stability, IEEE Trans. Appl. Supercond., 22(2012).

[16] W. Du, H. F. Wang, S. Cheng, J. Y. Wen, and R. Dunn, Robustness of damping control implemented by energy storage systems installed in power systems, Int. J. Electr. Power Energy Syst.,33(2011) 35-42.

[17] J. Shi, Y. J. Tang, Y. J. Xia, L. Ren, J. D. Li, and F. S. Jiao, Energy function based SMES controller for transient stability enhancement, IEEE Trans. Appl. Supercond., 22 (2012).

[18] J. K. Fang, W. Yao, Z. Chen, J. Y. Wen, and S. J. Cheng, Design of anti-windup compensator for energy storage-based damping controller to enhance power system stability, IEEE Trans. Power Syst., 29(2014) 1175-1185.

[19] A. H. M. A. Rahim, E. P. Nowicki, and O. P. Malik, Enhancement of power

system dynamic performance through an on-line self-tuning adaptive SVC controller, Electr. Power Syst. Res., 76(2006) 801-807.

[20] Q. H. Wu and B. W. Hogg, Robust self-tuning regulator for a synchronous generator, IEE Proc.-Control Theory Appl., 135(1988) 463-473.

[21] D. Rai, R. Gokaraju, and S. O. Faried, Adaptive control using constrained RLS and dynamic pole-shift technique for TCSCs, IEEE Trans. Power Delivery, 29(2014) 224-234.

[22] S. P. Azad, R. Iravani, and J. E. Tate, Damping inter-area oscillations based on a model predictive control (MPC) HVDC supplementary controller, IEEE Trans. Power Syst., 28(2013) 3174-3183.

[23] H. Ye and Y. T. Liu, Design of model predictive controllers for adaptive damping of inter-area oscillations, Int. J. Electr. Power Energy Syst., 45(2013) 509-518.

[24] D. W. Clarke, C. Mohtadi, and P. S. Tuffs, Generalized predictive control-part I: the basic algorithm, Automatica, 23 (1987) 137-148.

[25] V. Rajkumar and R. R. Mohler, Bilinear generalized predictive control using the thyristor-controlled series-capacitor, IEEE Trans. Power Syst., 9(1994) 1987-1993.

[26] E. Bijami, J. Askari, and M. M. Farsangi, Design of stabilising signals for power system damping using generalised predictive control optimised by a new hybrid shuffled frog leaping algorithm, IET Gener. Transm. Distrib., 6(2012) 1036-1045.

[27] J. A. L. Barreiros, A. S. e Silva, and A. J. A. Simoes Costa, A self-tuning generalized predictive power system stabilizer, Int. J. Electr. Power Energy Syst., 20 (1998) 213-219.

[28] A. Heniche and I. Kamwa, Control loops selection to damp inter-area oscillations of electrical networks, IEEE Trans. Power Syst., 17 (2002) 378-384.

[29] W. Yao, L. Jiang, J. Y. Wen, Q. H. Wu, and S. J. Cheng, Wide-area damping controller of FACTS devices for inter-area oscillations considering communication time delays, IEEE Trans. Power Syst., 29 (2014) 318-329.

[30] M. A. Pai, *Energy function analysis for power system stability*, Boston, MA: Kluwer, 1989.

[31] W. Yao, L. Jiang, J. Y.Wen, Q. H.Wu, and S. J. Cheng, Wide-area damping controller for power system inter-area oscillations: a networked predictive control approach, IEEE Trans. Control Syst. Technol., 23 (2015) 27-36.